

Article

GIS-Based Regional Seismic Risk Assessment for Dubai, UAE, Using NHERI SimCenter R2D Application

Ahmed Mansour Maky ¹, Mohammad AlHamaydeh ^{1,*} and Mona Saleh ²

¹ Department of Civil Engineering, College of Engineering, American University of Sharjah, Sharjah P.O. Box 26666, United Arab Emirates; b00089711@aus.edu

² Department of Civil Engineering, Faculty of Engineering, Aswan University, Aswan 81528, Egypt; monaesmail093@gmail.com

* Correspondence: malhamaydeh@aus.edu

Abstract: Over the last two decades, the UAE's construction sector has grown significantly with the development of tall buildings, but the region faces seismic risks. Similar concerns in China led to earthquake simulation research on a city scale. The objectives include developing programming for parallel computing and creating simplified models for estimating losses. The challenges include computational complexity and uncertainties in various modules. In 1995, the structural engineering community adopted performance-based engineering principles, shifting to a probabilistic design process. The Computational Modeling and Simulation Center (SimCenter) implemented this into a generic software platform, with the 2010 release of Regional Resilience Determination (R2D) automating the methodology. A research plan aims to advance realistic seismic simulation in the UAE, integrating studies and custom developments. The goal is to create an end-to-end seismic risk assessment framework aligned with digital trends, such as BIM and GIS. The investigation focuses on a virtual dataset for tall buildings, considering variations in location, material properties, height, and seismic activity. For the studied archetypes, the average expected losses include a 3.6% collapse probability, a 14% repair cost, 22 days repair time per asset, and almost 1.5% total population injuries, ranging from 1% for the lowest severity to 0.15% for the highest.



Citation: Maky, A.M.; AlHamaydeh, M.; Saleh, M. GIS-Based Regional Seismic Risk Assessment for Dubai, UAE, Using NHERI SimCenter R2D Application. *Buildings* **2024**, *14*, 1277. <https://doi.org/10.3390/buildings14051277>

Academic Editors: Claudia Brito De Carvalho Bello and Ingrid Boem

Received: 22 December 2023

Revised: 10 April 2024

Accepted: 15 April 2024

Published: 1 May 2024



Copyright: © 2024 by the authors. Licensee MDPI, Basel, Switzerland. This article is an open access article distributed under the terms and conditions of the Creative Commons Attribution (CC BY) license (<https://creativecommons.org/licenses/by/4.0/>).

1. Introduction

Since the beginning of 2010, there have been approximately 120 super-high-rise buildings taller than 300 m, based on a statistical inventory by the Council on Tall Buildings and Urban Habitat (CTBUH). This survey included either completed or under-construction tall buildings and determined that they are mainly located in regions with rapid economic development: China, UAE, and the USA (there are 47 in China, 28 in the UAE, and 18 in the USA). However, most developing cities are threatened by severe seismic disasters. This risk created a critical and motivational need to develop a scientific prediction of seismic damage platform, providing early warning of potential seismic risks. The main challenges consisted of (1) achieving precise flexural–shear deformations for each building with efficient computational techniques, which would require limited time, practical computational demand, and storage resources and (2) implementing a performance-based engineering framework, which would include all uncertainties and probabilistic inputs and present stakeholders' outputs, such as injuries and economic losses. The following paragraphs present the progress achieved by several studies on related objectives, such as implementing a more brilliant programming architecture to minimize computational costs and developing simplified numerical models to accurately reflect the inter-story earthquake damage with fewer DOFs.

1.1. Open-Source Packages for Regional Earthquake Simulations

A scientific workflow was proposed in order to provide an open-source platform and a standard architecture for solving regional hazard simulations and loss estimation problems [1]. Conceptually, the workflow is divided into a sequence of modules, where each one is determined to provide the resulting data based on defined inputs. This design allows for future developments or enhancements in modules. It can also smoothly replace the proposed applications with others while preserving the format of the inputs/outputs used in other models. The source code is published on the GitHub hosting platform. Some applications, programmed in C++ or Python, are provided for each module, while the data exchange through workflow modules is saved in JSON format. The definition of inputs, outputs, primary function, and available applications for each module, as well as the assumptions considered, are briefly plotted in Figure 1, which is adapted from [1].

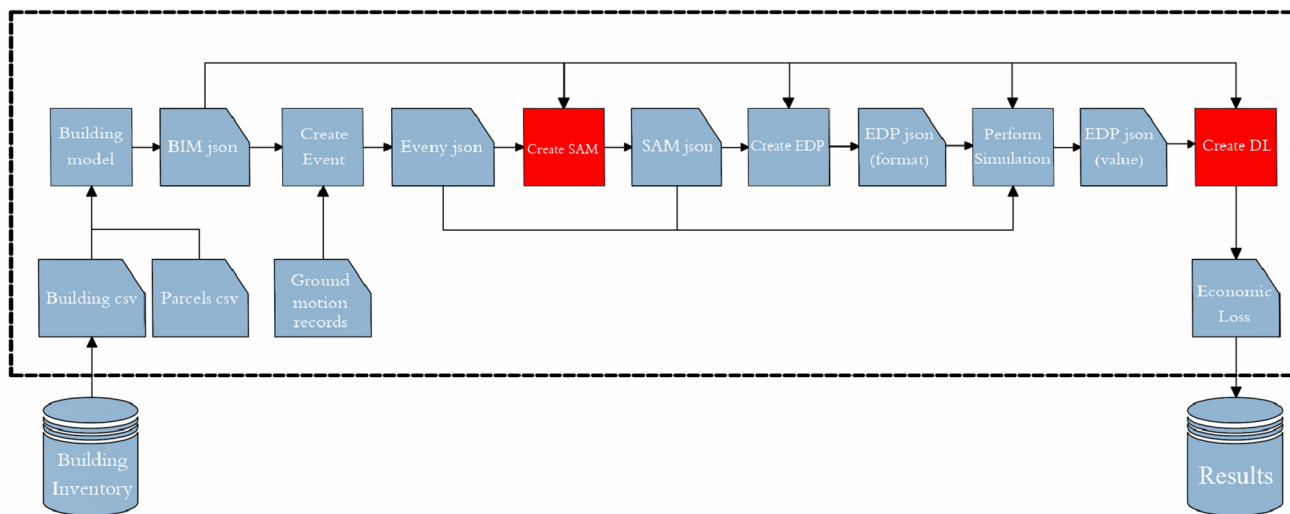


Figure 1. Scientific workflow for regional earthquake simulations, this figure is adapted from [1].

On 13 January 2021, the SimCenter team released the first version of the Regional Resilience Determination (R2D) tool [2], a graphical user interface for the SimCenter application framework. It facilitates defining the studied events, building databases, and visual representations of the maps and resulting DL ratios through integration with ESRI-ArcGIS SDK libraries. The application was designed with an architecture of two components: front-end user interface (UI) and back-end applications. The front end was developed using the cross-platform QT framework to generate user inputs in the local machine. However, the back end is an application workflow in C++ or Python, which processes the critical analysis on a remote server (a high-performance computer (HPC) utilizing the resources available through DesignSafe). This design utilizes cloud computing concepts, particularly for large datasets, which require specific computational resources and cannot fit with the available personal computer (PC) potentials. The user manual, downloading source configurations, and solved examples are available on their website [2,3].

1.2. UAE Seismicity Uncertainties

In recent years, the real estate sector in the UAE has witnessed significant development in the construction of tall buildings and iconic structures. Unfortunately, this area lacks data regarding seismic events and definitions of structural design considerations to be applied. Generally, the UAE is subjected to relatively high seismic risks, according to Table 1. The data in Table 1 is from [4,5]. Several studies indicate that, on average, three seismic events per year affect the UAE based on observations from 2000 to 2006. For example, a moderate earthquake ($M_b = 5$) shook a vast area in the northeast of UAE on 11 March 2002, and it was accompanied by smaller foreshocks and aftershocks [6]. On 27 November 2005 and 10 September 2008, more complex earthquakes with magnitudes of $M_b = 5.9$ and 6 started

in the Qeshm Island region in the Hormozgan province of southern Iran. Their impacts extended and were widely felt in northern UAE, leading to the evacuation of some areas. In addition, two local earthquakes (with $M_b = 3.7$ and 3.9) occurred in the eastern region of UAE on 10 March and 13 September 2007, respectively. In 2018, a seismic hazard analysis (SHA) study obtained many of the UAE's geophysical parameters, such as PGA, soil type, geology, slope, and fault line distance [7].

Table 1. The primary seismic risk sources in the UAE. The data is from [4,5].

Seismic Risk Source	Description
The Zagros Fold and Thrust Belt	A series of major blind thrust faults capable of generating $M_b \sim 7$ earthquakes.
The Makran Subduction Zone	A shallow dipping seismic source $\sim 6^\circ$, which steepens to $\sim 19^\circ$ south of Iran's coastline. It produced an $M_s = 8$ earthquake in 1945.
The Zendan-Minab Fault System	A complex faulting system created by the Makran subduction zone, joining the Zagros fold and thrust belt. It is capable of generating moderate/large earthquakes.
The Sabzevaran Jiroft Fault System	It has a similar seismogenic potential to the Zendan-Minab fault system, located further east.
Oman Mountains and the Dibba Line	The region exhibits features of faulting and a history of active tectonics. The 2002 Masafi earthquake originated in this region.
The West Coast Fault	It crosses the cities of Dubai and Abu Dhabi and passes very close to Ra's Al Khaymah. There is limited information regarding its activity (debatable existence).

The previous UAE seismic hazard investigation studies reported a high variation, from no seismic hazard to very high seismicity, as shown in Table 2. The data in Table 2 is from [8]. In 2006, the Dubai Seismic Network (DSN) [9] was established to record earthquakes from local and distant resources through four stations. From 2006 to 2014, many regional seismic activities were recorded from faults surrounding the UAE. Additionally, local seismic activities are noticed from three primary sources: (1) Masafi-Bani Hamid, (2) northern Huwaylat, and (3) Wadi-Nazw.

Table 2. Comparison of the results of Dubai seismic hazard studies [8].

Study	PGA (Return Period = 475 Years) (g)
Al-Haddad et al. [10]	<0.05
Abdalla and Al Homoud [11]	0.14
Peiris et al. [12]	0.06
Sigbjornsson and Elnashai [6]	0.16
Musson et al. [13]	0.05
Aldama-Bustos et al. [14]	<0.05
Shama [15]	0.17
Grunthel et al. [16]	0.32

The uncertainties in estimating the seismicity level in UAE regions caused ambiguity among designers regarding defining the analytical loads and the best practices for the statical systems and material properties. Several studies have been conducted in this area. In 2011, the seismic design factors were investigated in Ref. [17]—the response modification factor (R), the deflection amplification factor (C_d), and the system overstrength factor (Ω_0)—for three reference buildings designed in Dubai with four, sixteen, and thirty-two stories. The chosen structure system was RC special moment resisting frames, and two different sets of ground motions were applied corresponding to 475 and 2475 return periods. They concluded that the seismic design level significantly impacts the building R factor and

recommended period-dependent R and C_d Tables. In 2020, an investigation was performed by Ref. [18], referencing twelve archetypes of buildings, which included a variation in building height (6, 9, and 12 stories), design seismicity level (low, intermediate, and high), and type of shear wall (ordinary or special). They recommended being conservative in designing seismic intensity and utilizing the special RC shear walls for optimizing lateral behavior based on the probability of collapse and economic loss results. In 2022, three associated studies [19–21] compared the lateral performance of RC tall buildings with two layers of ductile coupled shear walls according to building heights (20, 40, and 60 stories), shear wall alignments, and concrete properties among normal concrete strengths and different ultra-high-performance concrete (UHPC) materials. The results showed a significant impact of UHPC on structure performance and total cost aspects.

2. Methodology and Research Significance

The GIS-based risk assessment study for Dubai in Ref. [22] could be considered the first step in UAE regional simulations. Heavy work was included in the data collection aspect, where Dubai was divided into several neighborhoods, and the dominating usage classified each area. Additionally, the number of buildings in each neighborhood was estimated approximately according to the population density. However, a more profound methodology will be implemented in this research as another advanced step toward an entirely realistic city-scale simulation. Significant changes are determined through all performance-based stages: hazard, structural, damage, and loss analyses. This research extensively reviews the literature regarding UAE seismicity, the effects of seismicity, performance-based earthquake engineering, and computing regional earthquake frameworks. The study aims to perform a virtual sample on a city scale using 17 reference models. The MCS model will be utilized for low-rise and medium-rise structures. The designed tall building models will be calibrated to an equivalent NMFS model to facilitate several simulations within regular PC capabilities. The R2D 2 [2] software package will be utilized to perform a regional seismic simulation. This package provides a graphical user interface (GUI) for an end-to-end regional earthquake framework, which includes all stages of a PBED process. It will be used to perform an earthquake scenario simulation for each grid in the UAE region to select the most likely earthquake record. The primary outputs are the damage cost and probability of collapse for each asset in the virtual database. As shown in Figure 2, the workflow can be organized into three major phases: (1) Earthquake scenario simulation: The studied region will be divided into grids, and an input ground motion will be assigned to each grid. The studied earthquake sources can be filtered according to the maximum distance and minimum and maximum magnitude. The ground motion record at each record is formulated from the included resources based on a “ground motion prediction equation”, such as that by Abrahamson, Silva, and Kamai (2014) [23]; (2) Assuming the buildings database: Many reference buildings should be selected according to the required variation. A high-fidelity FEM should be determined for non-linear analyses. These archetypes will be distributed on the map to simulate the neighborhoods’ usage; (3) Regional simulation: A non-linear dynamic analysis will be performed for each asset in the database by assigning the input ground motion to the closest earthquake grid. Then, a damage and loss analysis will be performed to relate the collapse probability, economic losses, and injuries to EDPs. All estimated data will be visualized on a GIS map to deduce the relationships between building parameters and loss outputs.

The research significance of the proposed study can be summarized as follows: (1) An “earthquake scenario simulation” will be performed for the hazard analysis stage instead of using reference records. This change would incorporate the effect of the location on the input ground motions for structural analysis. The region would be divided into 2D grids, and an input ground motion would be generated for each grid according to an earthquake prediction equation; (2) The structural analysis stage will include a more comprehensive range of archetypes. Seventeen archetypes will be adopted with a high variation in building height, from low-rise to high-rise (from single story to 50 stories),

and other building properties, such as occupancy; (3) The calibrated model concepts will be investigated in a structural analysis to achieve simulations with personal computer capabilities. The MCS model will simulate low-rise and mid-rise archetypes, while the NMFS model will be utilized for high-rise buildings; (4) The PEER PBEE methodology will be implemented and the HAZUS-MH 2.1 manual followed [24] in order to determine the collapse probability and DL parameters (such as monetary loss and injuries) for the included assets.

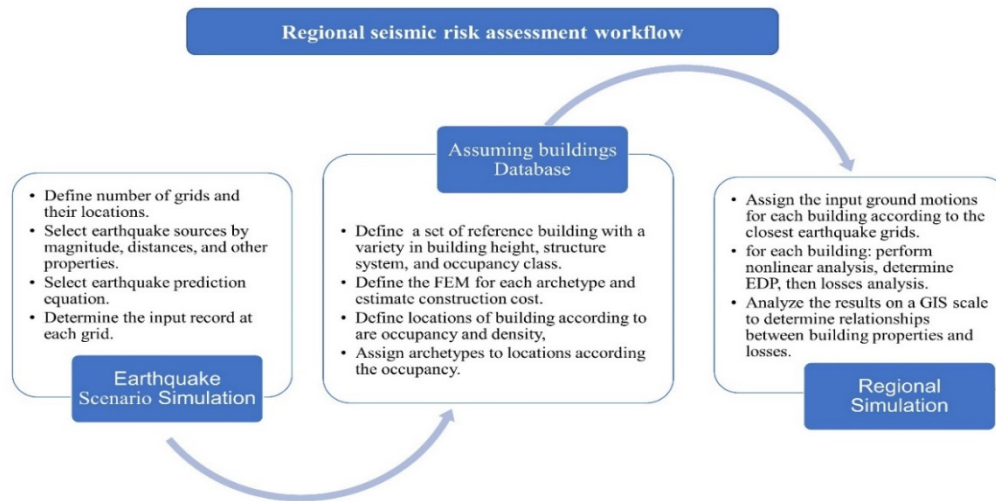


Figure 2. Flowchart for regional earthquake workflow.

Tables 3 and 4 demonstrate the parameters of the adopted reference buildings, where the cost of archetypes was estimated according to Ref. [25]. The authors classified them into five low-rise buildings, three mid-rise buildings, and nine high-rise buildings. The detailed FE element model is required to deduct the MCS model for low-rise and medium-rise buildings. Instead, a procedure was proposed in Ref. [1] to estimate the hysteresis parameters of each floor and implemented using R2D [2]. Three different elastic design response spectra were selected to simulate the ambiguity in defining the seismicity level. These spectra were defined in Ref. [26], and their key parameters are ($S_s = 0.18$ g, 0.42 g, and 1.65 g) and ($S_1 = 0.06$ g, 0.17 g, and 0.65 g) for low, medium, and high seismicity levels. The chosen models show a variation in structure systems, usage, and design seismic levels according to the common types in the UAE region. On the other hand, a detailed FE is required to calibrate the NMFS model for high-rise buildings [27]. Nine tall buildings are assumed to be commercial construction, with RC shear walls, from 2000 to 2010.

Table 3. Parameters of low-rise and medium-rise archetypes.

Label	Number of Stories	Year Built	Occupancy Class	Structure Type	Plan Area (Ft ²)	Cost (AED K)	Seismic Level
LR_RES_F1	1	1981	RES1	RM1L	1615	675	Low
LR_RES_F2	2	1995	RES3	C1L	2690	2025	Low
LR_RES_F3	3	2000	RES3	C2L	4300	4850	Low
MR_RES_F5	5	2002	RES3	C1L	5382	14,500	Middle
LR_COM_F3	3	1990	COM2	C1L	5920	7012	Low
MR_COM_F6	6	2005	COM1	C1L	5382	16,120	Middle
MR_COM_F7	7	2010	COM1	C2L	5382	18,805	Middle
LR_IND_F1	1	2003	IND2	S1L	10,764	4500	Middle

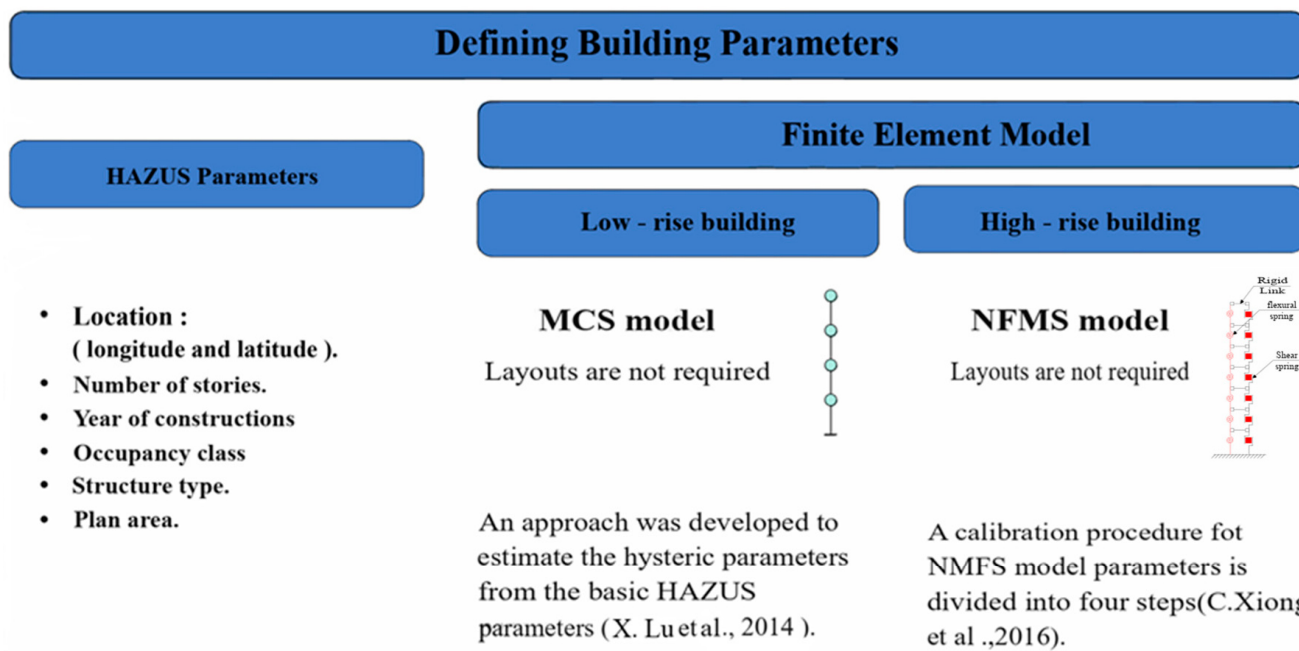
RES refers to residential occupancy; RES1 stands for a single family; RES3 stands for multiple families. COM refers to commercial occupation; COM1 and COM2 refer to retail trade and wholesale trade. IND2 indicates light industrial factory. RM1L, C1L, C2L, and S1L represent reinforced masonry bearing walls, concrete moment frames, concrete shear walls, and steel moment frames for the structure types.

Table 4. Parameters of high-rise archetypes.

Label	Number of Stories	Cost (AED)	Year Built	Material Properties		Plan Area (Ft ²)	Seismic Level
				F _{c'} (MPa)	F _y (MPa)		
HR_COM_F10	10	58,485					
HR_COM_F15	15	87,727	2000	50	420		
HR_COM_F20	20	115,970					
HR_COM_F25	25	146,211					
HR_COM_F30	30	175,454	2005	60	420	9685	High
HR_COM_F35	35	204,696					
HR_COM_F40	40	233,939					
HR_COM_F45	45	263,181	2010	70	500		
HR_COM_F50	50	292,423					

COM refers to commercial occupancy; COM4 stands for professional/technical services. C2L represents structures with concrete shear walls.

The reference buildings will be distributed in Dubai neighborhoods according to the usage and population density, and these data are available and published in Ref. [22]. Each grid's earthquake records will be selected according to the scenario simulation component in R2D [2]. A series of regional simulations will be executed for a differently designed model. The outputs are GIS maps for the collapse probability and economic loss. According to the total height and shear wall strength parameters, these maps will be a heuristic reference for designers. This research will represent the first-step stage of regional simulations in the UAE, where the distant goal is to collect and digitalize an actual building inventory database. Figure 3 illustrates the flowchart outlining the necessary data for defining a building [27,28].

**Figure 3.** Flowchart for the required data to define a building [27,28].

3. Calibrating NMFS Models for Tall Building Archetypes

3.1. Design of Tall Building Archetypes

The material properties and the number of floors of the selected high-rise buildings are shown in Table 4, while the unified floor layout and structural system are presented in

Figure 4. The columns of the building's structural grid are represented by (A, B, C, D, E, and F) along the X-axis and (1, 2, 3, 4, 5, and 6) along the Y-axis. The assumed layout is a double symmetric plan view for an office building comprising five 20 foot bays (6.0 m) in both north–south and east–west directions. The lateral resisting system consists of two shear wall layers (single shear walls in the edge perimeter and double shear walls connected with coupling beams in interior axes). For the slabs, the f'_c is assumed to be 4.0 ksi (28 MPa). Additionally, the associated loads are defined as per ASCE7-16 [29]: 42.5 psf (2.036 kPa) for the superimposed load (SDL), 7.5 psf (0.359 kPa) for the curtain wall (cladding) on the perimeter of each floor, 50 psf (2.394 kPa) for the typical floors' live load, 20 psf (0.958 kPa) for roof live loads, and the self-weight of the concrete slabs. The soil classification for the site will be taken as "D" as the code recommends when no specific soil exploration information is available.

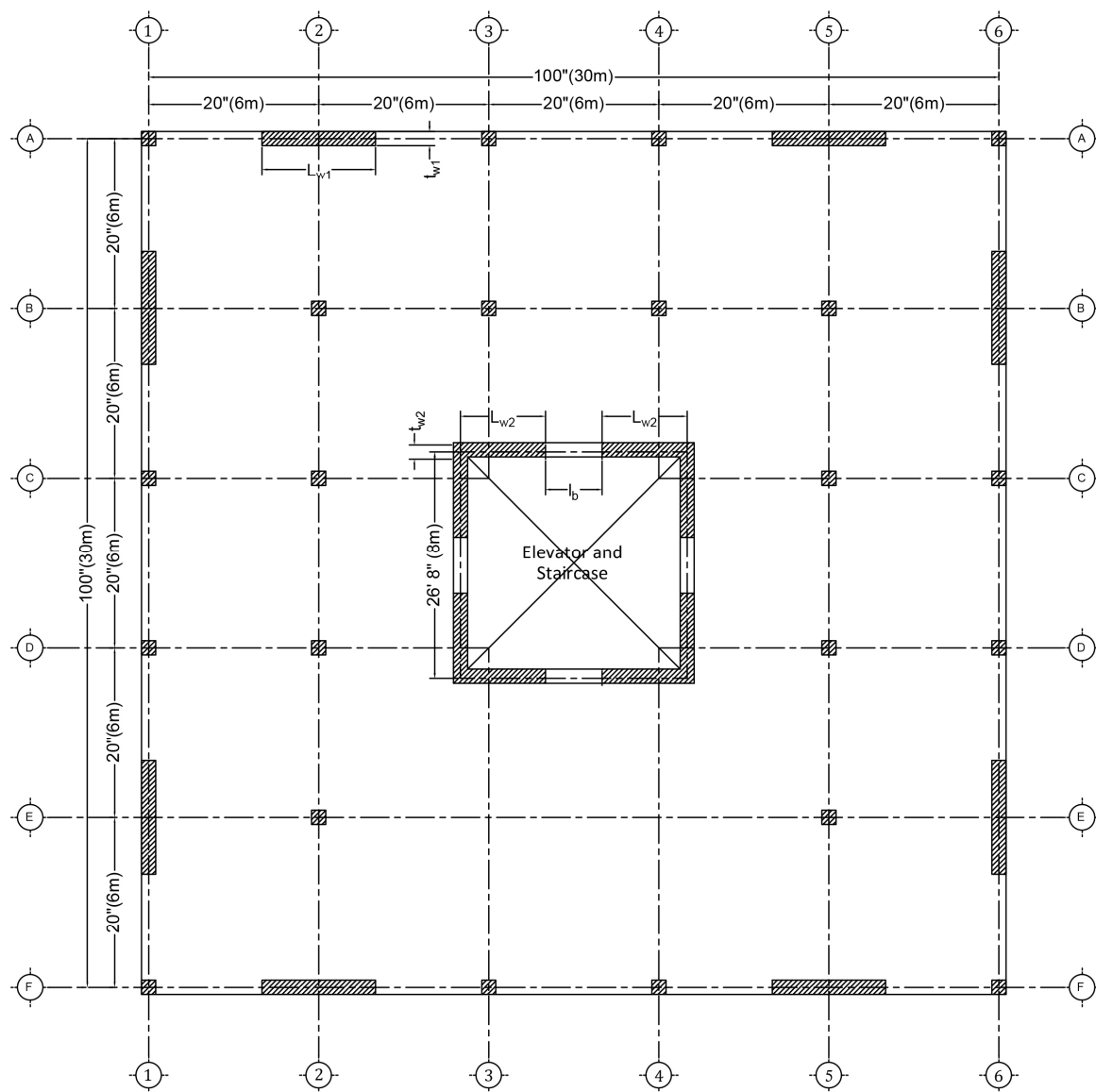


Figure 4. Typical floor plan view for tall building archetypes.

3.2. Calibration Resulting Model (Calibrating NMFS Models for Tall Building Archetypes)

A trial heuristic algorithm was implemented to determine the best values for NMFS model parameters, which achieve the closest pushover curve to the detailed FE models. The main optimization criteria consisted of reducing the mean squared error between the two curves. The final values for Ω_y , Ω_p , and μ are reported in Table 5. Numerically, the

relative errors for peak strength and total curve area were 0.02, 0.08 for the worst cases, less than 1.0×10^{-5} , with 0.04 as the average. Meanwhile, the MSE estimations were below 0.006 and had an average value of 0.004. The efficiency of using NMFS is clarified, as the time required for the simplified models represents only 4/1000 of the computational time required for the detailed models, on average. Specifically, this is the ratio between 3/1000 and 6/1000.

Table 5. Estimated parameters for NMFS models.

Archetype	NMFS Model Parameters				
	Ω_y	Ω_p	μ	EI (KN·m ⁴)	GA (KN·m ²)
M1_10F_50RC	2.65	1.20	5.28	1.7×10^8	1.2×10^6
M2_15F_50RC	1.25	1.25	6.11	1.4×10^8	5.9×10^5
M3_20F_50RC	1.62	1.24	2.36	2.9×10^8	4.7×10^5
M4_25F_60RC	1.22	1.23	2.41	3.8×10^8	3.8×10^5
M5_30F_60RC	1.06	1.24	2.28	1.1×10^9	3.1×10^5
M6_35F_60RC	1.25	1.26	1.83	4.5×10^9	3.4×10^5
M7_40F_70RC	1.30	1.26	2.01	7.3×10^9	3.5×10^5
M8_45F_70RC	1.24	1.27	1.40	4.3×10^9	2.7×10^5
M9_50F_70RC	1.13	1.27	1.40	6.2×10^9	2.4×10^5
Average	1.41	1.25	2.80	2.7×10^9	4.6×10^5

4. GIS Databases for Buildings, Ground Motions, and Risk Assessment Results

4.1. Input Ground Motions

As shown in Table 1, the UAE is surrounded by regional and local seismic geological resources. The “earthquake scenario simulation” component in R2D [2] was utilized to generate input ground motions. Multiple-point-earthquake sources, which were collected from different resources to represent the surrounding seismic resources [30–32], were defined, as listed in Table 6. An input ground motion was estimated at each neighborhood’s representative location (longitude and latitude) corresponding to every seismic source using Chiou and Youngs’ prediction equation [30].

Table 6. Properties of earthquakes included in an earthquake simulation scenario.

Location	Date	Longitude	Latitude	M_w	Focal Depth (km)
Chaldoran	24 November 1976	39.07	44.38	7.0	15
Tabas	16 September 1978	33.60	56.93	7.4	11
KuliBonyabad	27 November 1979	30.67	51.60	7.0	25
Sirch	28 July 1981	30.20	57.54	7.2	15.5
ArdekulGhaen	10 May 1997	34.61	49.85	7.2	10
Manjil	6 November 1990	28.25	55.46	7.4	11
Hormozgan, northwest of Dehbarez	2000	27.56	56.84	4.2	41
Hormozgan, northwest of Dehbarez	2002	27.64	56.74	5.3	12
Hormozgan, northeast of Bandar-e Abbas	2002	27.49	56.62	4.4	33
Masafi-Bani Hamid	13 September 2007	25.46	56.2	4.0	20

4.2. Buildings Database

This study included 17 archetypes representing different occupancy classes, number of stories, and design seismicity levels. Dubai was segmented into 221 neighborhoods [22], and for each one, the number of buildings was estimated approximately according to the population density. In addition, every area was classified according to its primary occupancy into residential, commercial, industrial, and unidentified. In order to estimate the number of archetype buildings in a specific area, the archetypes were grouped according to the occupancy class and a close number of stories. Then, hypothetical distribution ratios were defined to represent each group out of the total buildings in each neighborhood, as shown in Table 7.

Table 7. Hypothetical distribution ratios for archetypes in different neighborhood classes.

Archetype Group	Description	Stories	Neighborhood Class			
			Residential	Commercial	Industrial	Unidentified
RES (1_5)	Low- and medium-rise residential buildings	1–5	0.50	0.00	0.30	0.40
IND	Light industrial buildings	1	0.00	0.00	0.70	0.10
COM (3_7)	Low- and medium-rise commercial buildings	3–7	0.25	0.25	0.15	0.15
COM (10_20)	High-rise commercial buildings	10–20	0.15	0.25	0.00	0.15
COM (25_35)	High-rise commercial buildings	25–35	0.05	0.25	0.00	0.10
COM (40_50)	High-rise commercial buildings	40–50	0.05	0.25	0.00	0.10

5. Risk Assessment Results

The simulation process included three forms of inputs, which were assigned two spatial attributes: ground motions, the buildings database, and FE scripts for MCS and NMFS models. Meanwhile, Figures 5–10 display the results, including the expected collapse probability and losses for each building. The results are encapsulated in different scales: (1) overall studied city; (2) neighborhoods; (3) neighborhood classes; (4) archetype groups; and (5) archetypes. R2D [2] utilizes the PELICUN [31] package for the FEMA-P58 methodology to determine the decision variables. FEMA developed a method for determining collapse probability by developing fragility curves. The fragility functions are calibrated using various analytical, experimental, and simulation methods. The analytical methods use mathematical equations to calculate the collapse probability of a building based on the engineering demand parameters (EDPs), material properties, and asset classifications.

5.1. Collapse Probability

The results can be summarized as follows: The collapse probability for the modeled buildings can differ from 0.00% to 60%, with a mean value of almost 4%. The “LR_RES_F1” archetype represents the highest collapse probability ratio, which is slightly less than 8%, while the lowest ratio is 0.00%, expected for the “LR_IND_F1” archetype, as shown in Figure 5c. The expected collapse ratios for concrete structures range from 3% to 8%, 1.2% to 3.5%, and 0.2% to 2.3% for low-rise, medium-rise, and high-rise archetypes, respectively. In other words, “RES (1_5)” is the highest archetype group, with an expected collapse probability of 5.5%. The collapse probability for commercial concrete structures decreases with respect to height from 3% for “COM (3_7)” to 0.2% for “COM (40_50)”, as shown in Figure 5b. As expected, residential neighborhoods have the highest mean collapse probability of almost 4%, and commercial neighborhoods have the lowest ratio of 0.8%, while the ratios for industrial and unidentified neighborhoods are 1.8% and 3.1%, as represented in Figure 5a, respectively. Projecting these results on a GIS scale leads to the choropleth map shown in Figure 10a, determining the mean collapse probability for Dubai’s neighborhoods.

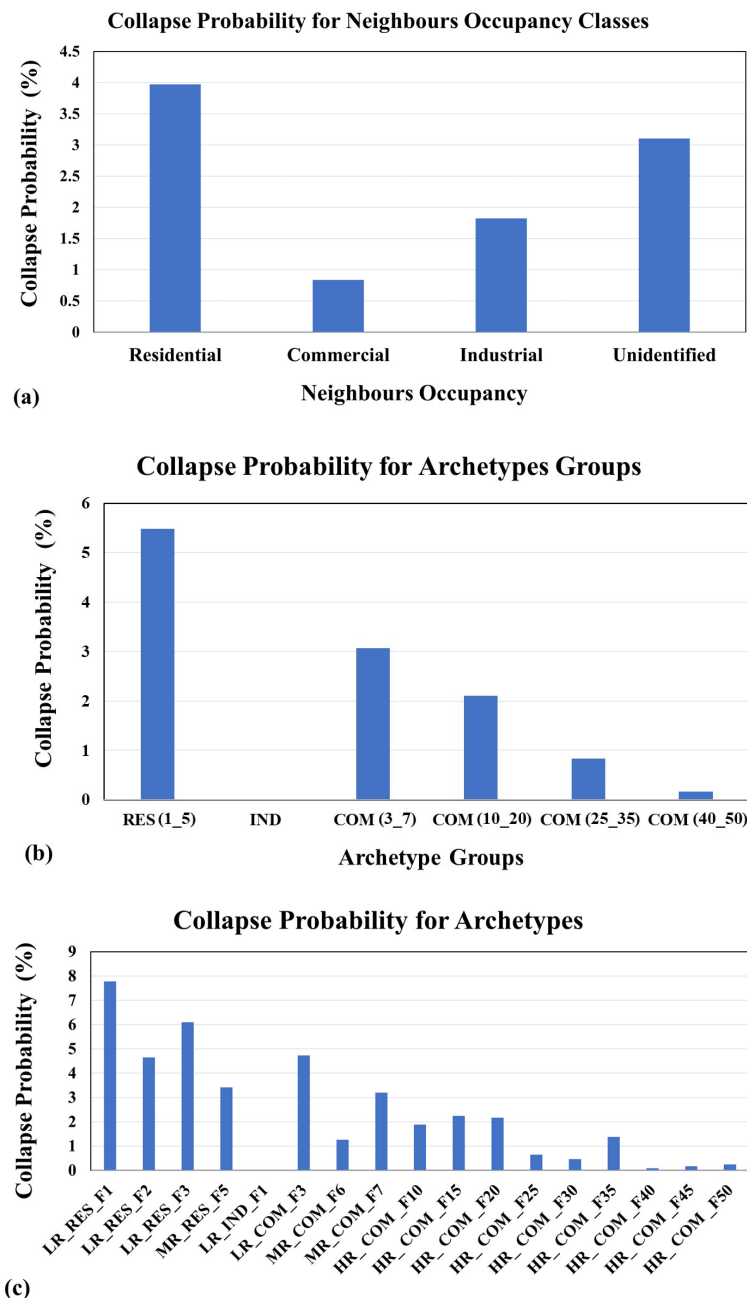


Figure 5. Mean values of the estimated collapse probability: (a) Neighborhood classes, (b) Archetype groups, and (c) Archetypes.

5.2. Repair Cost–Replacement Cost Ratio

The monetary losses due to replacement or repair are a factual parameter in assessing earthquake disasters, which depends on the collapse probability, construction material (steel, concrete, etc.), and the structure system. These factors are reflected in the estimations as follows. The highest archetype for the repair cost–replacement cost ratio is the single-story masonry building “LR_RES_F1”, with 28%, followed by the light-steel industrial structure “LR_IND_F1”, with 26%, as shown in Figure 6c. The average ratio for residential archetypes is 21%, and for commercial archetype groups, it ranges from 12% for the “COM (3_7)” group to 2% for the “COM (40_50)” group, as represented in Figure 6b. For the GIS scale, the average losses for neighborhood classes can be ordered in a descending order of industrial (23%), residential (15%), unidentified (11.5%), and commercial (4.5%) (see Figure 6a). Additionally, the expected losses per individual neighborhood are represented

in Figure 10b, which vary from 0% to 35%. Finally, the average cost for the cumulative city is expected to be 14%, accompanied by a 0.25 standard deviation.

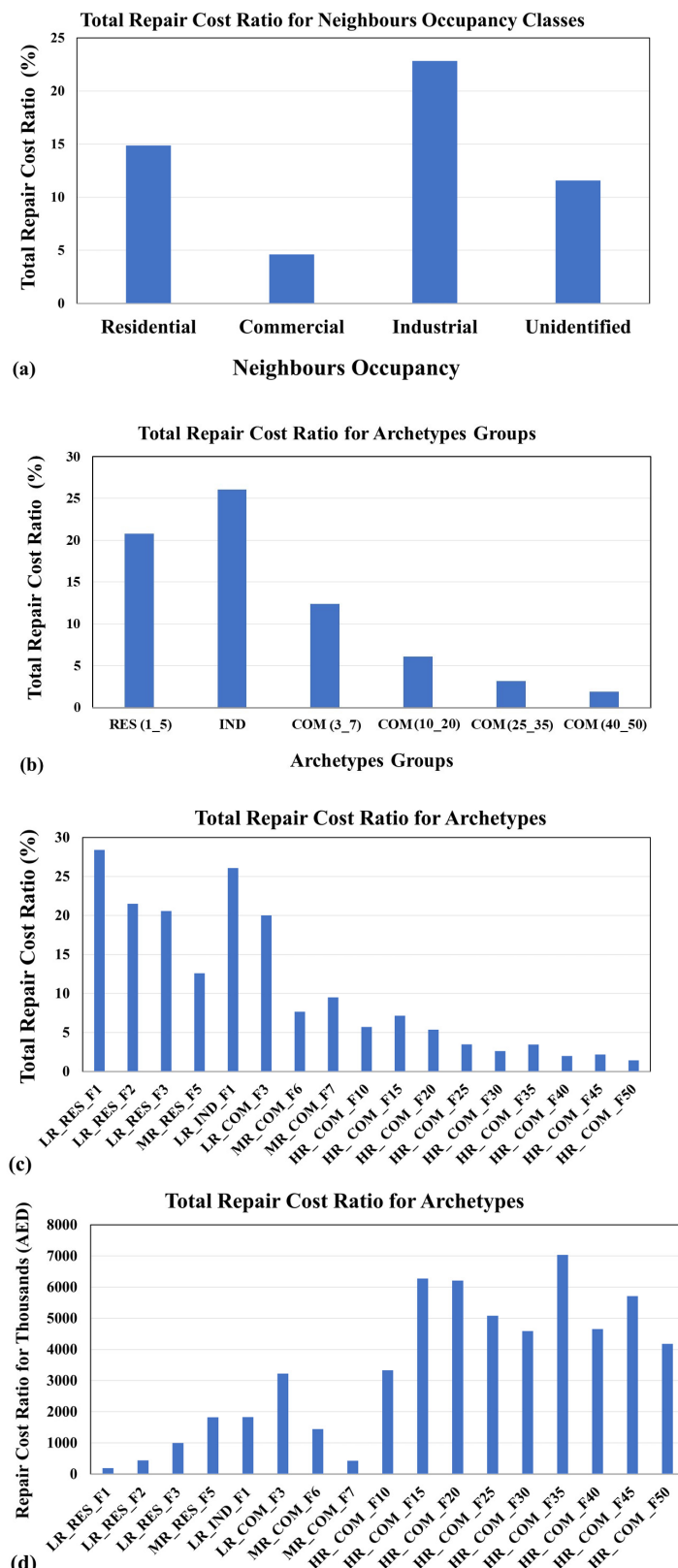


Figure 6. Mean values of estimated repair cost-replacement cost ratio: (a) Neighborhood classes; (b) Archetype groups; (c) Archetypes; (d) Archetype repair cost in thousands AED.

5.3. Repair Time

Like the repair cost, the required repair time is related to construction materials and the structural system. Figure 7d clarifies that the “LR_IND_F1” archetype requires the greatest number of days for repairs (223 days for the mean value), with a significant difference to other archetypes. “LR_RES_F1” is the second highest archetype in terms of repair time, with 29 days associated with a standard deviation of 49. The average number of days required for concrete archetype repair is 25 for low-rise, 16 for medium-rise, and 4–25 for high-rise buildings. As presented in Figure 7c, the average repair days required for residential archetypes is 25 days, and for the commercial archetype groups, the range is from 18 days for the “COM (3_7)” group to 6 days for the “COM (40_50)” group. Figure 7b shows the repair time probabilities for different neighborhood classes. The mean values can be ordered in a descending order of industrial (148 days), unidentified (48 days), residential (20 days), and commercial (11 days). The overall estimated probability is 22 days, associated with a standard deviation of 52, as shown in Figure 7a. Finally, Figure 10c includes the choropleth map for the expected repair time for the studied neighborhoods in the form of a colored scale from 0 to 220 days.

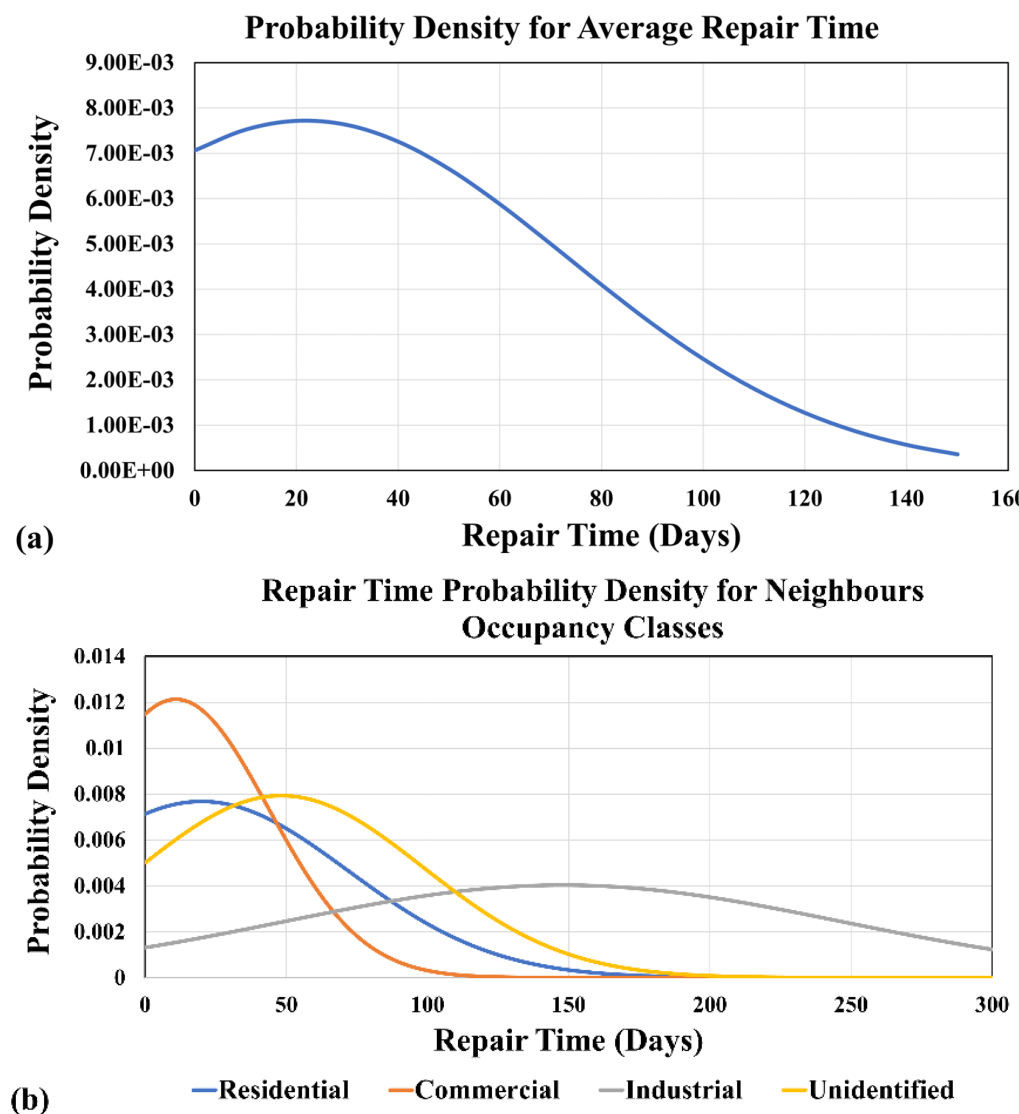


Figure 7. Cont.

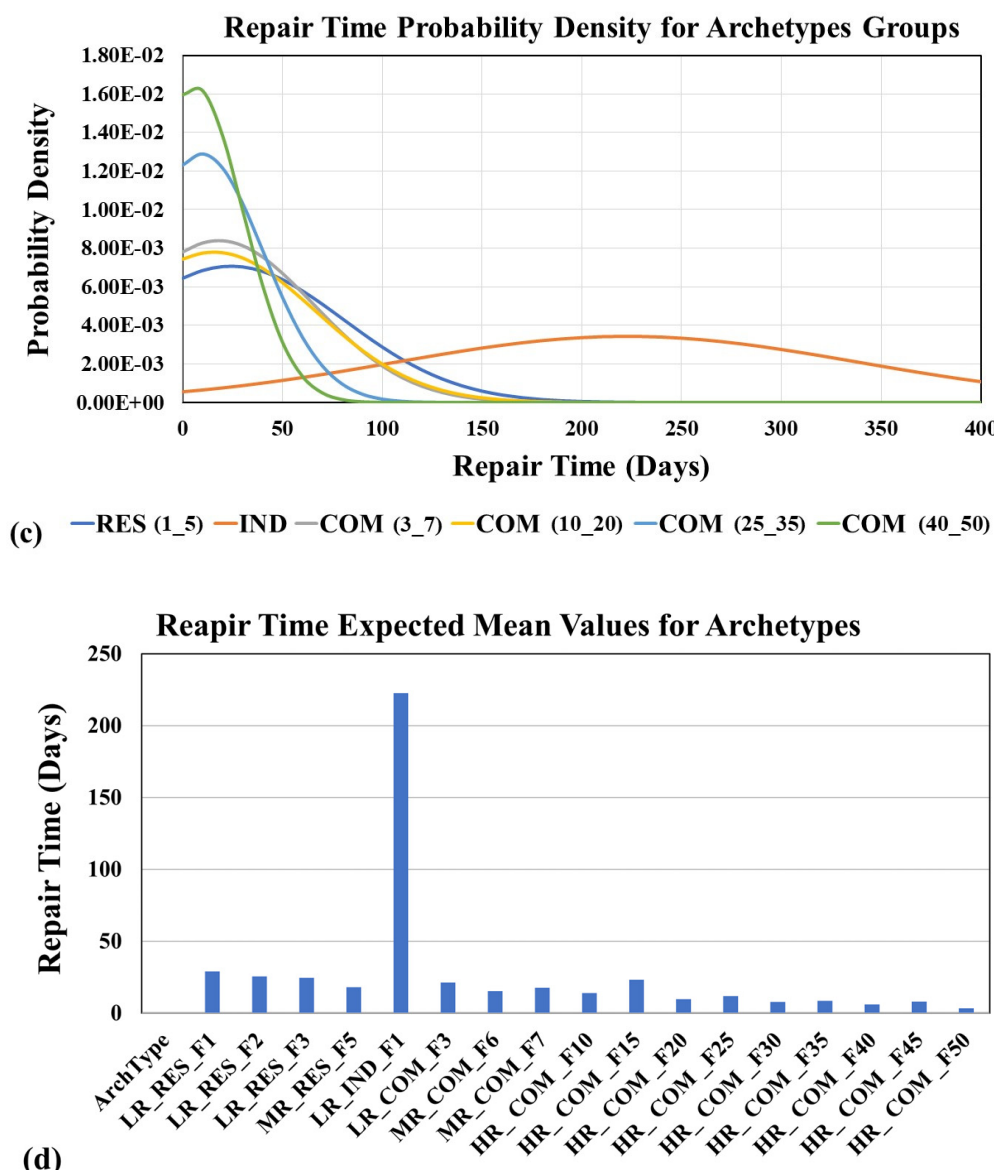


Figure 7. Estimated repair time as a probability density: (a) Overall assets; (b) Neighborhood classes; (c) Archetype groups; and (d) Mean values of archetypes.

5.4. Injuries

The expected injuries of the total occupancy population are classified in an ascending order of severity, from one to four. The estimated injuries are summarized as follows. The mean total injuries for the studied region are approximately 1.5% of the population; 62% represents the lowest severity, while 10% represents the highest severity (see Figure 8a). As a result of the collapse probabilities and expected damage variables, the expected average injuries range from 1.7% to 6.5% for low-rise archetypes, from 0.2% to 5.3% for medium-rise archetypes, and from 0.04% to 0% for high-rise archetypes, as shown in Figure 9. The “LR_RES_F1” archetype has the highest total injuries, with 6.5%, distributed as 83%, 16.5% for the first and second severity, and 0.02% for the third and fourth severity. This is followed by the “LR_IND_F1” archetype, with 5%. The ratios of the injuries’ severity are 60%, 24%, 5%, and 10%, from lowest to highest. Meanwhile, for concrete models, the total injuries are 2% for the worst severity, 61% for the lowest severity, and 10% for the highest severity. The mean values for neighborhood classes can be ordered in a descending order of industrial (4.1%), residential (1.6%), unidentified (1.1%), and

commercial (0.1%) (see Figure 8b). Finally, a representative map of the injuries distributed per studied neighborhood can be found in Figure 10d.

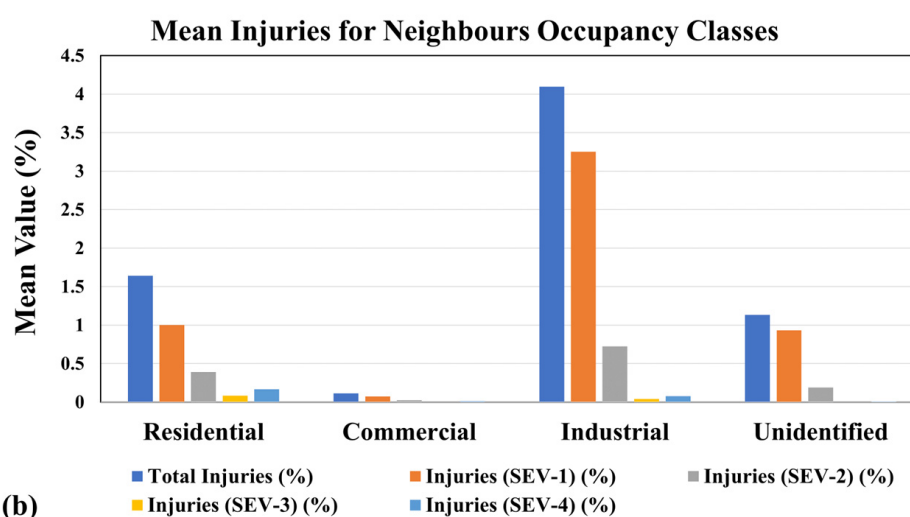
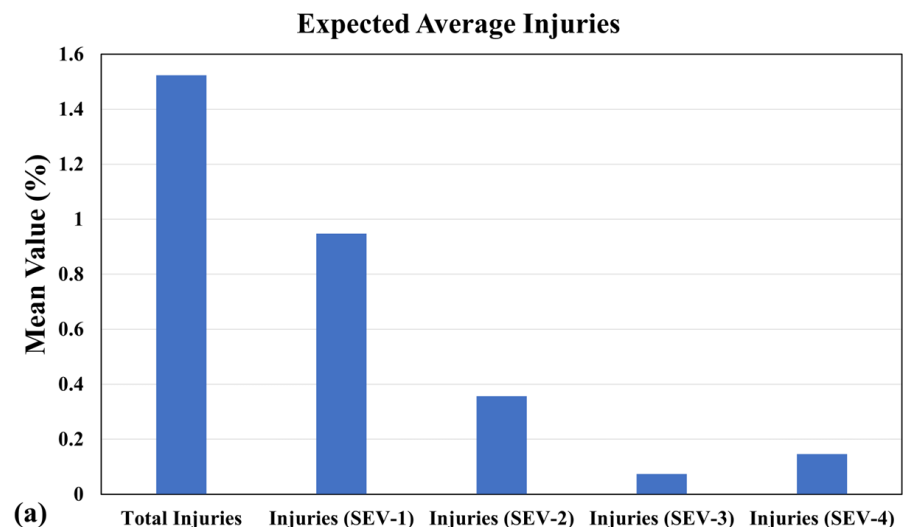


Figure 8. Mean values of estimated injuries: (a) Overall averages; and (b) Neighborhood classes.

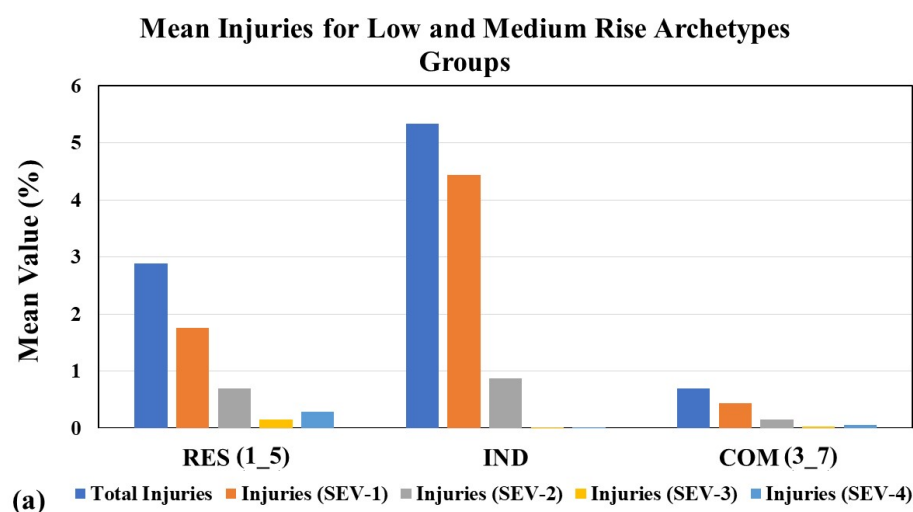


Figure 9. Cont.

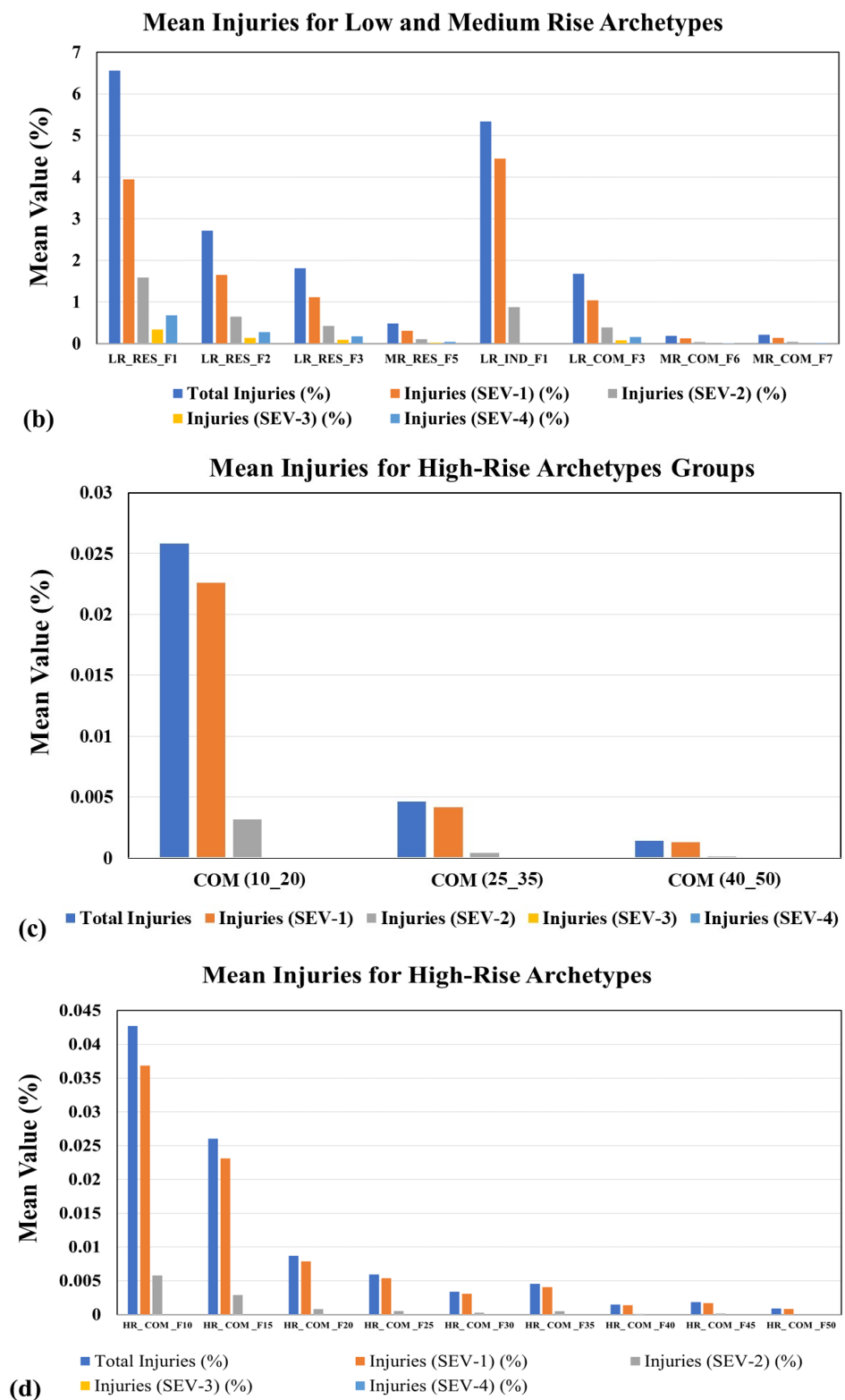


Figure 9. Mean values of estimated injuries: (a) Low- and medium-rise archetype groups; (b) Low- and medium-rise archetypes; (c) High-rise archetype groups; and (d) High-rise archetypes.

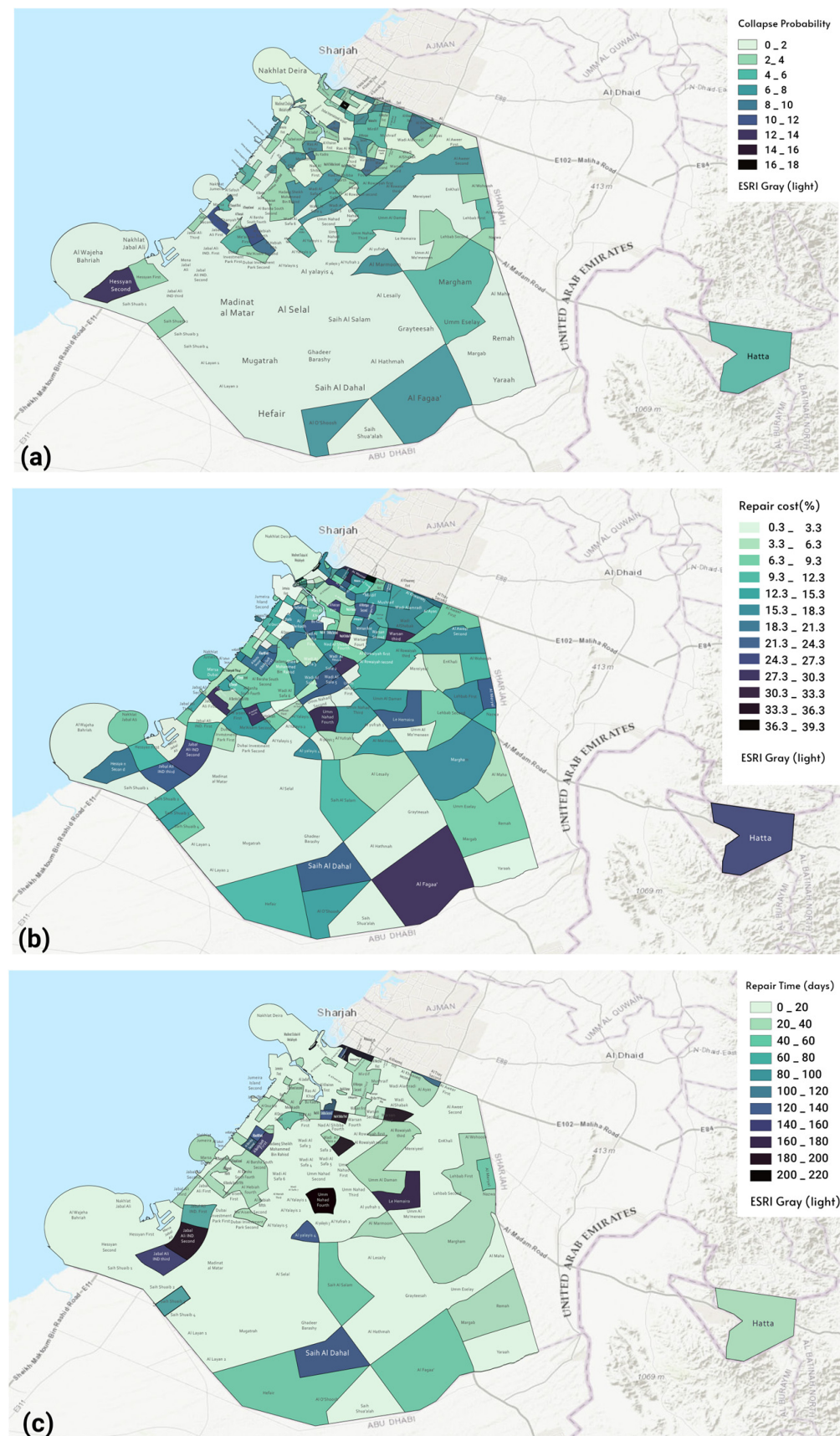


Figure 10. Cont.

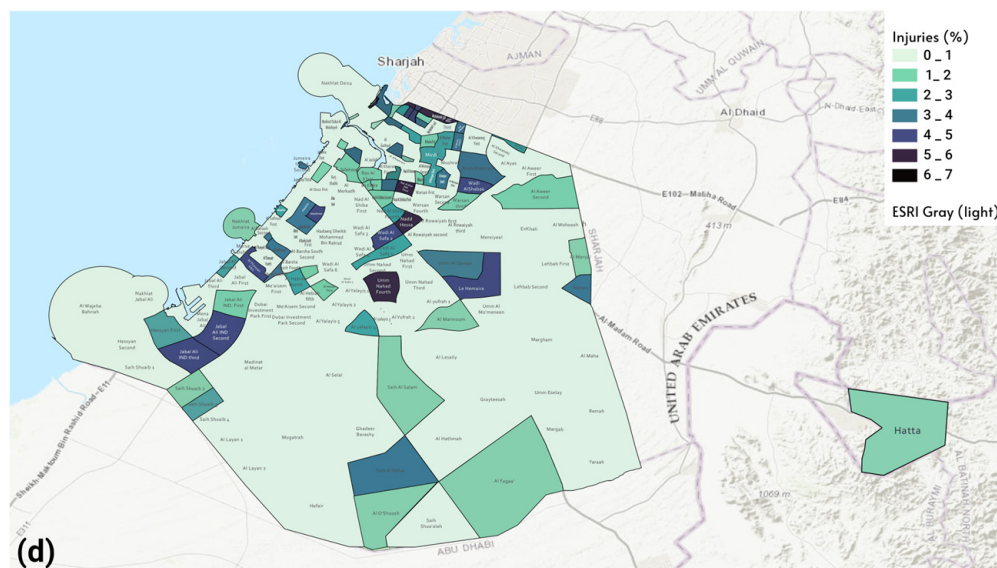


Figure 10. GIS choropleth maps representative of loss variables: (a) Collapse probability; (b) Repair cost; (c) Repair time; (d) Injuries.

6. Conclusions

The conclusion based on the configured outputs for the studied archetypes is as follows. The “LR_RES_F1” and “LR_IND_F1” archetypes exhibit different results and patterns from those of other archetypes. “LR_RES_F1” is a bearing masonry wall residential house built more than 40 years ago for a single family. “LR_IND_F1” is a steel moment-framing structure for a light industrial purpose constructed almost 20 years ago, while other archetypes represent concrete structures for residential or commercial assets. “LR_RES_F1” produces the highest collapse probability of 8%, a repair cost of 28%, and total injuries of 6.5%. Despite the “LR_IND_F1” being the lowest archetype in terms of collapse probability (equaling zero), it produces the second highest repair cost and total injury losses (26% and 5%, respectively). Moreover, it represents the longest repair time at 223 days, with a significant difference to other models (second longest repair time equaling 29 days). The seismic design spectrum is the key factor in scaling all loss parameters. The archetypes designed under the assumption of low seismic intensity had a collapse probability range from 4.6% to 8%, repair cost from 20% to 28.5%, and total injuries from 1.7% to 6.6%. For medium-rise archetypes, these results decrease from 1.3% to 3.4% for collapse probability, from 9.5% to 12.6% for repair cost, and from 0.2% to 5.3% for injuries. Archetypes designed for a high seismic intensity achieved the lowest loss values: from 0.2% to 2.3%, from 1.4% to 7%, and from 0.04% to 0% for collapse probability, repair cost, and injuries, respectively.

The neighborhood occupancy results were obtained according to the estimated number of assets and the assumed archetype distribution weights. The residential neighborhoods possess the highest collapse probability estimation. They have an expected collapse probability of 4%, a repair cost-replacement cost ratio of 15%, an average of 20 days expected for repairs, and total injuries of 1.6% (1%, 0.4%, 0.08%, and 0.2% for different severity levels, in an ascending order). The average expected collapse probability for commercial buildings is 0.8%. Their estimated repair costs and time are 4.6% and 11 days. The expected total injuries are only 0.1%, 65% for the lowest severity and 9% for the worst cases. The industrial areas possess the highest values for loss variables, except for the collapse probability, which is 2%. Their estimated repair costs and time are 23% and 148 days. The expected total injuries are 4%, 79% for the lowest severity and only 2% for the worst cases. For neighborhoods with undefined classifications, the estimated loss variables are a collapse probability of 3%, a repair cost-replacement cost ratio of 11.6%, an average of 48 days expected for repairs, and total injuries of 1.1% (0.9%, 0.2%, 0.00%, and 0.01% for different severity levels, in an ascending order). Finally, the overall expected losses, as average values, are a collapse

probability of 3.6%, a repair cost of 14% of the total replacement cost, a repair time of 22 days for each asset, and total injuries of almost 1.5% of the total population. The injuries differ from lowest to highest severity at 1%, 0.4%, 0.07%, and 0.15%, respectively.

This research continues a study published in 2022 [22] toward the long-term goal of developing seismic regional simulation databases for UAE cities, which represent reality with high confidence. The authors emphasize that this kind of project is critically needed because of the unique characteristics of massive construction growth in recent years, with high uncertainty regarding seismic activities throughout the same period. According to the available data, the current phase only represents prototypal results based on the assumed archetypes. However, considerable effort should be made in data collection and computational development to reach the full reality simulation. This maturity in data understanding can be reflected in urban planning, disaster management, and stakeholders when determining the maintenance cost for a single facility or neighborhood corresponding to the selected location, construction materials, and the number of floors. Additionally, these digital datasets can be used to train and verify artificial intelligence algorithms for urban planning, transportation, and infrastructural simulations, e.g., Refs. [32–34].

Future Research Trends and Priorities for Regional Seismic Risk Assessment (SRA):

- The future of SRA research lies in improving the treatment and propagation of uncertainties in scenario-based and probabilistic risk assessments [35].
- There is a need for advancements in the methodological development of regional SRA, including hazard analysis, exposure modeling, fragility assessment, and consequence evaluation, as well as the associated uncertainty quantification and propagation [36].
- Developing resilience metrics, restoration modeling, and planning in regional seismic resilience assessment is also a priority for future research in SRA [37].
- Current Challenges in Regional SRA Research:
 - The lack of review studies summarizing the research advancements in SRA from a regional-level perspective presents a challenge in understanding the methodological developments and limitations in regional SRA [36].
 - The complexity introduced by regional-level assessment—which includes additional dimensions and complexity compared to traditional site-specific assessment—poses challenges in SRA research [36].
- Role of Machine Learning and AI in Regional SRA Research:
 - Machine learning and AI can be leveraged for regional SRA by integrating these technologies in assessing seismic hazard impacts, vulnerability modeling, and consequence evaluation, thereby improving the quantitative and probabilistic assessment of regional seismic hazard impacts [36].
 - The use of machine-learning algorithms in seismic vulnerability assessment can effectively protect against earthquakes, as demonstrated in a case study in a densely populated urban area near an active fault [37].
- Key Factors Influencing Research Priorities in Regional SRA:
 - The potential implications of seismic risk for disaster management and urban planning, especially in densely populated urban areas, influence the research priorities in regional SRA [38].
 - Considering the complexity and uncertainty involved, the need for a systematic approach to reliably and realistically address the risk of seismic events also influences the research priorities in regional SRA [39].

Potential Implications of Regional SRA Research for Disaster Management and Urban Planning:

- Regional SRA research has implications for the production of seismic risk maps, which are valuable tools for planning mitigation measures to improve the level of preparedness in case of an earthquake, especially in urban areas [38].
- The deployment of seismic risk management, informed by regional SRA, can support resiliency planning and prioritization of seismic retrofit projects for spatially distributed critical infrastructure, such as water and wastewater systems [40].

Author Contributions: Conceptualization, M.A.; methodology, M.A.; software, A.M.M.; validation, A.M.M. and M.A.; formal analysis, A.M.M. and M.A.; investigation, M.A., A.M.M. and M.S.; resources, M.A.; data curation, A.M.M.; writing—original draft preparation, A.M.M.; writing—review and editing, M.A. and M.S.; visualization, A.M.M., M.A. and M.S.; supervision, M.A.; project administration, M.A.; funding acquisition, M.A. All authors have read and agreed to the published version of the manuscript.

Funding: This research was financially supported by the American University of Sharjah (AUS) through the Open Access Program (OAP). The authors greatly appreciate this financial support. This paper represents the opinions of the authors and does not intend to represent the position or opinions of the AUS.

Data Availability Statement: All data, models, or code generated or used during the study are available in a repository or online in accordance with funder data retention policies.

Acknowledgments: The authors appreciate and acknowledge Ahmed Elkady's involvement in this research. The authors greatly appreciate the financial support from AUS. This paper represents the opinions of the authors and does not intend to represent the position or opinions of the AUS.

Conflicts of Interest: The authors declare no conflicts of interest.

References

1. Lu, X.; McKenna, F.; Cheng, Q.; Xu, Z.; Zeng, X.; Mahin, S.A. An open-source framework for regional earthquake loss estimation using the city-scale nonlinear time history analysis. *Earthq. Spectra* **2020**, *36*, 806–831. [[CrossRef](#)]
2. McKenna, F.; Gavrilovic, S.; Zhao, J.; Zhong, K.; Zsarnoczay, A.; Cetiner, B.; Yi, S.-R.; Arduino, P.; Elhaddad, W. The Regional Resilience Determination (R2D). 2021. Available online: <https://nheri-simcenter.github.io/R2D-Documentation/index.html> (accessed on 21 May 2021).
3. SimCenter. Available online: <https://simcenter.designsafe-ci.org/> (accessed on 30 September 2022).
4. International Seismological Centre. *Disaster Prev. Manag. Int. J.* **1992**, *8*, 452. [[CrossRef](#)]
5. National Geoscience Database of IRAN. 2011. Available online: <http://www.ngdir.ir/Earthquake/Earthquake.asp> (accessed on 21 May 2021).
6. Sigbjornsson, R.; Elnashai, A.S. Hazard assessment of Dubai, united arab emirates, for close and distant earthquakes. *J. Earthq. Eng.* **2006**, *10*, 748–773. [[CrossRef](#)]
7. Al-Dogom, D.; Schuckma, K.; Al-Ruzouq, R. Geostatistical seismic analysis and hazard assessment; United Arab Emirates. *Int. Arch. Photogramm. Remote Sens. Spat. Inf. Sci. ISPRS Arch.* **2018**, *42*, 29–36. [[CrossRef](#)]
8. Al Khatibi, E.; Elenean, A. Dubai Seismic Network. Dubai Municipality. 2012, p. 2460. Available online: <https://www.seismo.geodesy.ae/dsn.aspx> (accessed on 9 April 2021).
9. Khan, Z.; El-Emam, M.; Irfan, M.; Abdalla, J. Probabilistic seismic hazard analysis and spectral accelerations for United Arab Emirates. *Nat. Hazards* **2013**, *67*, 569–589. [[CrossRef](#)]
10. Al-Haddad, M.; Siddiqi, G.H.; Al-Zaid, R.; Arafah, A.; Necioglu, A.; Turkelli, N. A Basis for Evaluation of Seismic Hazard and Design Criteria for Saudi Arabia. *Earthq. Spectra* **1994**, *10*, 231–258. [[CrossRef](#)]
11. Abdalla, J.A.; Al-Homoud, A.S. Seismic hazard assessment of United Arab Emirates and its surroundings. *J. Earthq. Eng.* **2004**, *8*, 817–837. [[CrossRef](#)]
12. Peiris, N.; Free, M.; Lubkowski, Z.; Hussein, A.T. Seismic hazard and seismic design requirements for the Arabian Gulf region. In Proceedings of the First European Conference on Earthquake Engineering and Seismology, Geneva, Switzerland, 3–8 September 2006; Volume 10.
13. Musson, P.M.W.; Northmore, K.J.; Sargeant, S.; Phillips, E.; David, B.; David, L.; McCue, K.; Ambraseys, N.N. *The Geology and Geophysics of the United Arab Emirates Volume 4: Geological Hazards*; Abu Dhabi, Ministry of Energy, United Arab Emirates: Abu Dhabi, United Arab Emirates, 2006; Volume 4, p. 251.
14. Aldama-Bustos, G.; Bommer, J.J.; Fenton, C.H.; Stafford, P.J. Probabilistic seismic hazard analysis for rock sites in the cities of Abu Dhabi, Dubai and Ra's Al Khaymah, United Arab Emirates. *Georisk* **2009**, *3*, 1–29. [[CrossRef](#)]
15. Shama, A.A. Site specific probabilistic seismic hazard analysis at Dubai Creek on the west coast of UAE. *Earthq. Eng. Eng. Vib.* **2011**, *10*, 143–152. [[CrossRef](#)]
16. Grünthal, G.; Bosse, C.; Sellami, S.; Mayer-Rosa, D.; Giardini, D. Compilation of the GSHAP regional seismic hazard for Europe, Africa and the Middle East. *Ann. Geophys.* **2021**, *42*, 2021. [[CrossRef](#)]
17. AlHamaydeh, M.; Abdullah, S.; Hamid, A.; Mustapha, A. Seismic design factors for RC special moment resisting frames in Dubai, UAE. *Earthq. Eng. Eng. Vib.* **2011**, *10*, 495–506. [[CrossRef](#)]
18. Aly, N.; AlHamaydeh, M.; Galal, K. Quantification of the Impact of Detailing on the Performance and Cost of RC Shear Wall Buildings in Regions with High Uncertainty in Seismicity Hazards. *J. Earthq. Eng.* **2020**, *24*, 421–446. [[CrossRef](#)]

19. AlHamaydeh, M.; Elkafrawy, M.E.; Aswad, N.G.; Talo, R.; Banu, S. Evaluation of UHPC Tall Buildings in UAE with Ductile Coupled Shear Walls under Seismic Loading. In Proceedings of the 2022 Advances in Science and Engineering Technology International Conferences (ASET), Dubai, United Arab Emirates, 21–24 February 2022; pp. 1–6. [CrossRef]
20. AlHamaydeh, M.; Elkafrawy, M.E.; Amin, F.M.; Maky, A.M.; Mahmoudi, F. Analysis and Design of UHPC Tall Buildings in UAE with Ductile Coupled Shear Walls Lateral Load Resisting System. In Proceedings of the 2022 Advances in Science and Engineering Technology International Conferences (ASET), Dubai, United Arab Emirates, 21–24 February 2022; pp. 1–6. [CrossRef]
21. AlHamaydeh, M.; Elkafrawy, M.; Banu, S. Seismic Performance and Cost Analysis of UHPC Tall Buildings in UAE with Ductile Coupled Shear Walls. *Materials* **2022**, *15*, 2888. [CrossRef]
22. AlHamaydeh, M.; Al-Shamsi, G.; Aly, N.; Ali, T. Geographic Information System-Based Seismic Risk Assessment for Dubai, UAE: A Step toward Resilience and Preparedness. *Pract. Period. Struct. Des. Constr.* **2022**, *27*, 04021069. [CrossRef]
23. Abrahamson, N.A.; Silva, W.J.; Kamai, R. Update of the AS08 Ground-Motion Prediction equations based on the NGA-west2 data set. In *Pacific Engineering Research Center Report*; Pacific Earthquake Engineering Research Center: Berkeley, CA, USA, 2013; Volume 174.
24. Hazus. *Hazus—MH 2.1: Technical Manual*; Federal Emergency Management Agency: Washington, DC, USA, 2012; Volume 718.
25. UAE Construction Cost Insight Report UAE Projects Snapshot. Jll-Mena. 2021. Available online: <https://www.jll-mena.com/en/trends-and-insights/research/the-uae-construction-market-report> (accessed on 22 March 2022).
26. AlHamaydeh, M.; Aly, N.; Galal, K. Effect of Diverse Seismic Hazard Estimates on Design and Performance of RC Shear Wall Buildings in Dubai, UAE. In Proceedings of the 2015 World Congress on Advances in Structural Engineering and Mechanics (ASEM15), Incheon, Republic of Korea, 25–29 August 2015.
27. Xiong, C.; Lu, X.; Guan, H.; Xu, Z. A nonlinear computational model for regional seismic simulation of tall buildings. *Bull. Earthq. Eng.* **2016**, *14*, 1047–1069. [CrossRef]
28. Lu, X.; Han, B.; Hori, M.; Xiong, C.; Xu, Z. A coarse-grained parallel approach for seismic damage simulations of urban areas based on refined models and GPU/CPU cooperative computing. *Adv. Eng. Softw.* **2014**, *70*, 90–103. [CrossRef]
29. American Society of Civil Engineers (ASCE). *Prestandard and Commentary for the Seismic Rehabilitation of Buildings*; FEMA-356; American Society of Civil Engineers: Washington, DC, USA, 2000.
30. Chiou, B.S.-J.; Youngs, R.R. Chiou and Youngs PEER-NGA Empirical Ground Motion Model for the Average Horizontal Component of Peak Acceleration and Pseudo-Spectral Acceleration for Spectral Periods of Interim Report for USGS Review. *PEER Rep. Draft. Pac. Earthq. Eng. Res. Cent. Berkeley CA* **2006**, 219. Available online: https://apps.peer.berkeley.edu/research/lifelines/nga_docs/jul_10_06/Chiou_Youngs_NGA_2006.pdf (accessed on 17 April 2023).
31. Zsarnóczay, A.; Deierlein, G.G. PELICUN—A Computational Framework for Estimating Damage, Loss and Community Resilience. In Proceedings of the 17th World Conference on Earthquake Engineering, Sendai, Japan, 13–18 September 2020; pp. 1–12.
32. Shen, Y.; Zhang, D.; Wang, R.; Li, J.; Huang, Z. SBD-K-medoids-based long-term settlement analysis of shield tunnel. *Transp. Geotech.* **2023**, *42*, 101053. [CrossRef]
33. Mohammed, D.; Horváth, B. Steady-Speed Traffic Capacity Analysis for Autonomous and Human-Driven Vehicles. *Appl. Sci.* **2023**, *14*, 337. [CrossRef]
34. Wang, D.; Lu, C.-T.; Fu, Y. Towards Automated Urban Planning: When Generative and ChatGPT-like AI Meets Urban Planning. *arXiv* **2023**, arXiv:2304.03892. Available online: <http://arxiv.org/abs/2304.03892> (accessed on 12 April 2023).
35. Crowley, H. Earthquake Risk Assessment: Present Shortcomings and Future Directions. *Perspect. Eur. Earthq. Eng. Seismol.* **2014**, *1*, 515–532. [CrossRef] [PubMed]
36. Du, A.; Wang, X.; Xie, Y.; Dong, Y. Regional seismic risk and resilience assessment: Methodological development, applicability, and future research needs—An earthquake engineering perspective. *Reliab. Eng. Syst. Saf.* **2023**, *233*, 109104. [CrossRef]
37. Narjabafam, P.; Hoseinpour, R.; Noori, M.; Altabay, W. Practical seismic resilience evaluation and crisis management planning through GIS-based vulnerability assessment of buildings. *Earthq. Eng. Eng. Vib.* **2021**, *20*, 25–37. [CrossRef]
38. Rasulo, A.; Fortuna, M.A.; Borzi, B. A seismic risk model for Italian urban areas. Safety and Reliability of Complex Engineered Systems. In Proceedings of the 25th European Safety and Reliability Conference, ESREL 2015, Zürich, Switzerland, 7–10 September 2015; pp. 4319–4326. [CrossRef]
39. Vahdat, K.; Smith, N.J.; Amiri, G. Seismic risk management: A system-based perspective. *Risk Manag.* **2014**, *16*, 294–318. [CrossRef]
40. Taing, J.; Nisar, A.; Hitchcock, C.S.; Bates, M.; Blackmun, R. Regional-scale seismic vulnerability assessment of medium-sized water and wastewater systems. *Lifelines* **2022**, *1*, 440–447. [CrossRef]

Disclaimer/Publisher’s Note: The statements, opinions and data contained in all publications are solely those of the individual author(s) and contributor(s) and not of MDPI and/or the editor(s). MDPI and/or the editor(s) disclaim responsibility for any injury to people or property resulting from any ideas, methods, instructions or products referred to in the content.